

Great enhancement of Curie temperature and magnetic anisotropy in two-dimensional van der Waals magnetic semiconductor heterostructures

Xue-Juan Dong¹, Jing-Yang You¹, Zhen Zhang¹, Bo Gu^{2,3,*} and Gang Su^{2,3,†}

¹ School of Physical Sciences, University of Chinese Academy of Sciences, Beijing 100049, China

² Kavli Institute for Theoretical Sciences, and CAS Center for Excellence in Topological Quantum Computation, University of Chinese Academy of Sciences, Beijing 100190, China

³ Physical Science Laboratory, Huairou National Comprehensive Science Center, Beijing 101400, China

(Dated: September 2, 2020)

In two-dimensional (2D) magnetic systems, large magnetic anisotropy is needed to stabilize the magnetic order according to Mermin-Wagner theorem. Based on density functional theory (DFT) calculations, we propose that the magnetic anisotropic energy (MAE) of 2D ferromagnetic (FM) semiconductors can be strongly enhanced in van der Waals heterostructures by attaching a non-magnetic semiconductor monolayer with large spin-orbit coupling. We studied Cr₂Ge₂Te₆/PtSe₂ bilayer heterostructures, where each layer has been realized in recent experiments. The DFT calculations show that the MAE of Cr₂Ge₂Te₆/PtSe₂ is enhanced by 70%, and the Curie temperature T_C is increased far beyond room temperature. A model Hamiltonian is suggested to analyze the DFT results, showing that both the Dzyaloshinskii-Moriya interaction and the single-ion anisotropy contribute to the enhancement of the MAE. Based on the superexchange picture, we find that the decreased energy difference between 3d orbitals of Cr and 5p orbitals of Te contributes partially to the increase of T_C . Our present work indicates a promising way to enhance the MAE and T_C by constructing van der Waals semiconductor heterostructures, which will inspire further studies on the 2D magnetic semiconductor systems.

I. INTRODUCTION

To achieve room temperature ferromagnetic semiconductors has long been an important topic in science [1]. Recently, magnetism in two-dimensional (2D) van der Waals materials has become a hot-spot which could lead to new device applications in information storage and spintronics [2–4]. People have devoted to explore 2D van der Waals ferromagnetic semiconductors, such as Cr₂Ge₂Te₆ [5], CrI₃ [6], Fe₃GeTe₂ [7], VSe₂ [8], MnSe₂ [9], and FePS₃ [10, 11], etc. These layered materials have enriched the database of 2D ferromagnetic materials, but there are still challenges ahead. On one hand, large magnetic anisotropic energy (MAE) is required to suppress the thermal fluctuations and to stabilize the 2D magnetic moment according to Mermin-Wagner theorem [12]. Different pictures, for instance, Kitaev interaction, single-ion anisotropy (SIA) [13] and p-d covalency [13] have been suggested to understand the MAE in 2D van der Waals ferromagnetic semiconductors. The Kitaev interaction and the SIA are originated from the spin-orbit coupling (SOC), the latter as a relativistic effect is usually small in many materials. On the other hand, high Curie temperature T_C above room temperature is very required from practical applications [14]. The Curie temperature of Cr₂Ge₂Te₆ bilayer and CrI₃ monolayer is 28 K and 45 K, respectively, far below room temperature [5, 6]. Efforts have been paid to enhance the magnetization of 2D van der Waals magnets and to seek for new 2D magnetic material as well as to control the magnetism

using mechanic and electronic means [15, 16]. Strain is another useful way to control the magnetism in 2D ferromagnetic semiconductors. For example, T_C in Cr₂Ge₂Se₆ monolayer can be increased beyond room temperature by applying just a few percent tensile strain [17], and the MAE of CrI₃ monolayer can also be tuned by strain [18].

It is known that combining two kinds of 2D materials into heterostructures could regulate the overall performance [19–22], which can thus provide platforms to study interfaces and device applications [23–25]. Van der Waals heterostructures are found to be an exotic platform that could realize fascinating phenomena [26–29]. The emergence of 2D magnetic materials has facilitated to explore more functional heterostructures, e.g. multiferroicity [30] and tunable electronic structure [31].

In WSe₂/CrI₃ heterostructures, the degenerate valleys in WSe₂ are split due to the proximity effect, where a large magnetic field of 13 T can be obtained by means of the ferromagnetic layer CrI₃ [32]. The chiral edge state is manipulated by constructing WTe₂/bilayer CrI₃/WTe₂ heterostructures, in which CrI₃ was used to magnetize the topological insulator WTe₂ [33]. In FeI₂/In₂Se₃ heterostructures, it is found that FeI₂ could undergo phase transition from ferromagnetic to antiferromagnetic (AFM) phase when the direction of ferroelectric polarization of In₂Se₃ is reversed [34]. Strong magnetic proximity effect via the s-d exchange coupling was proposed at the InAs/(Ga,Fe)Sb interface [35]. The effect of magnetic field on magnetic properties of metallic heterostructures Fe₃O₄/Pt was also studied [36]. The lattice mismatch is important for constructing heterostructures in experiments, and the epitaxial methods were often applied to produce van der Waals for highly lattice-mismatched systems [37]. The heterostructures with large lattice mis-

* gubo@ucas.ac.cn

† gsu@ucas.ac.cn

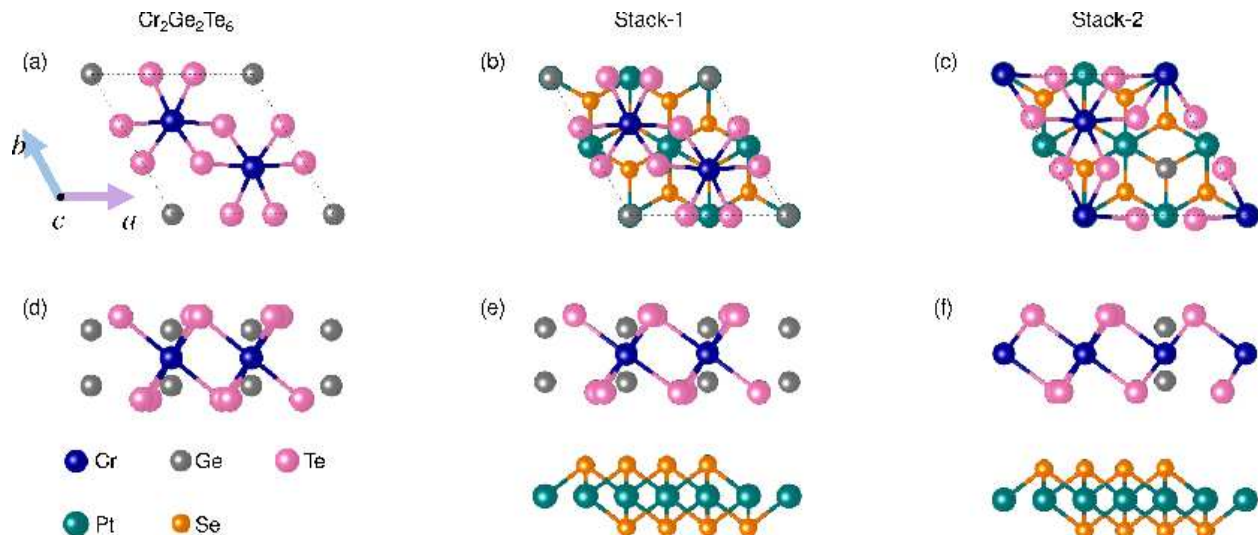


FIG. 1. Crystal structures of two-dimensional $\text{Cr}_2\text{Ge}_2\text{Te}_6$ and $\text{Cr}_2\text{Ge}_2\text{Te}_6/\text{PtSe}_2$ heterostructures with Stack-1 and Stack-2, (a)-(c): top view; (d)-(f) side view, respectively.

match about 10% can be realized in the experiments. For example, the heterostructures $\text{GaSe}/\text{MoSe}_2$ with lattice mismatch of 13% [38] and $\text{FeSe}/\text{Bi}_2\text{Te}_3$ with lattice mismatch of 19% [39] were realized in recent experiments.

By constructing 2D van der Waals semiconductor heterostructures, is it possible to enhance the MAE and T_C of ferromagnetic semiconductors? To answer this question, in this work, in terms of first principles calculations, we propose an efficient way to enhance the MAE and T_C of $\text{Cr}_2\text{Ge}_2\text{Te}_6$, through constructing van der Waals heterostructures with nonmagnetic PtSe_2 . Both $\text{Cr}_2\text{Ge}_2\text{Te}_6$ and PtSe_2 are 2D van der Waals semiconductors that have already been fabricated in experiments [5, 40]. We consider two stack configurations and find the Curie temperatures T_C of two stacks are larger than 600 K, while the MAE is increased by 70%. We present a model and show that both the Dzyaloshinskii-Moriya interaction and the SIA contribute to the enhancement of the magnetic anisotropy. The increase of T_C is partially owing to the decreased energy difference between 3d orbitals of Cr and 5p orbitals of Te. Our work will inspire further studies to enhance the magnetic properties of low-dimensional magnetic materials with the help of 2D van der Waals heterostructures. Considering the great progress of 2D van der Waals stacking structures in recent experiments, such as the van der Waals stacking-dependent interlayer [41], and general synthesis of 2D van der Waals heterostructure arrays [42], our present proposal will be readily feasible for experiments.

II. CALCULATION METHODS

We perform first principles calculations using Vienna *ab initio* simulation package (VASP) [43]. Spin-polarized calculations are conducted with the Perdew-

Burke-Ernzerhof exchange-correlation function and the generalized-gradient approximation. We adopted the DFT-D2 method of Grimme to describe the van der Waals interaction between $\text{Cr}_2\text{Ge}_2\text{Te}_6$ and PtSe_2 layers [44]. Spin-orbit coupling is taken into account in the calculations. $5 \times 5 \times 1$ and $3 \times 3 \times 1$ Mohnkhorst-Pack k -mesh sampling grids are used for the unit cell and supercell, respectively. The vacuum length is taken as 20 Å, which is enough to isolate the present 2D system. The in-plane supercell is taken as $\sqrt{3} \times 1$ in a rectangular shape. The Hubbard U for 3d electrons of Cr is chosen as 4 eV, which should be reasonable [17]. We relaxed the structure of $\text{Cr}_2\text{Ge}_2\text{Te}_6$ and PtSe_2 to obtain the ground-state structure. Based on the DFT results, the Curie temperature is calculated by using the Monte Carlo simulations [45] based on the 2D Ising model, where a 60×60 supercell is adopted, and 10^5 steps are performed for every temperature to acquire the equilibrium.

III. $\text{CR}_2\text{GE}_2\text{TE}_6/\text{PTSE}_2$ HETEROSTRUCTURES AND ENHANCEMENT OF MAGNETISM

Bulk $\text{Cr}_2\text{Ge}_2\text{Te}_6$ has been synthesized in 1995 [46] and successfully exfoliated into layers recently [5]. The space-group of 2D $\text{Cr}_2\text{Ge}_2\text{Te}_6$ is $\text{P}\bar{3}1\text{m}$ (No.162). Monolayer PtSe_2 is considered as the most appropriate candidate to combine with 2D $\text{Cr}_2\text{Ge}_2\text{Te}_6$, which is a semiconductor with a lattice constant of 3.76 Å that is well matched with the lattice of $\text{Cr}_2\text{Ge}_2\text{Te}_6$ and can be obtained by mechanical exfoliation methods [40]. The space group of PtSe_2 is $\text{P}\bar{3}1\text{m}$ (No. 164), very similar to that of $\text{Cr}_2\text{Ge}_2\text{Te}_6$. The heterostructure is constructed in such a way that monolayer PtSe_2 with a size of 2×2 is attached to monolayer $\text{Cr}_2\text{Ge}_2\text{Te}_6$ with a size of 1×1 . The lattice mismatch between $\text{Cr}_2\text{Ge}_2\text{Te}_6$ and PtSe_2 is 10%,

TABLE I. The DFT results of lattice parameter and electronic and magnetic properties of considered $\text{Cr}_2\text{Ge}_2\text{Te}_6$ with various lattice constants, and $\text{Cr}_2\text{Ge}_2\text{Te}_6/\text{PtSe}_2$ heterostructures with Stack-1 and Stack-2 obtained by the GGA + SOC + U calculations, where $U = 4$ eV.

	$\text{Cr}_2\text{Ge}_2\text{Te}_6$				$\text{Cr}_2\text{Ge}_2\text{Te}_6/\text{PtSe}_2$	
	Expt.	Expt. lat.	Relax lat.	Strain lat.	Stack-1	Stack-2
lattice (Å)	6.83	6.83	6.96	7.22	7.22	7.22
band gap (eV)	-	0.03	0.14	0.36	0.39	0.45
E_{FMz} (eV)	-	-44.5662	-44.6458	-44.4594	-109.3624	-109.2307
E_{FMx} (eV)	-	-44.5650	-44.6445	-44.4575	-109.3601	-109.2284
E_{AFM} (eV)	-	-44.4953	-44.5399	-44.3027	-109.1711	-109.0484
$S_d(\mu_B)(\text{Cr})$	-	3.59	3.52	3.66	3.59	3.68
MAE (meV)	-	1.19	1.33	1.89	2.32	2.23
T_C (K)	28	30	200	464	693	625

which could be executable in experiment for 2D van der Waals materials heterostructures [19]. We propose two ways to make the heterostructures named as Stack-1 and Stack-2, in both configurations PtSe_2 is located under $\text{Cr}_2\text{Ge}_2\text{Te}_6$. In Stack-1, the center of $\text{Cr}_2\text{Ge}_2\text{Te}_6$ unit cell and the $2 \times 2 \text{PtSe}_2$ is aligned in c direction, while Stack-2 can be treated as Stack-1 translating $\text{Cr}_2\text{Ge}_2\text{Te}_6$ layer with $1/3$ unit cell along $[1\ 2\ 0]$ direction. The space-group for Stack-1 and Stack-2 structures is P3 (No.143). The crystal structure of monolayer $\text{Cr}_2\text{Ge}_2\text{Te}_6$ and the two stacks are shown in Fig. 1. It is noted that the lattice constant becomes 7.22 Å for the heterostructure $\text{Cr}_2\text{Ge}_2\text{Te}_6/\text{PtSe}_2$, which is equivalent to applying 3.7% tensile strain to monolayer $\text{Cr}_2\text{Ge}_2\text{Te}_6$.

The properties of $\text{Cr}_2\text{Ge}_2\text{Te}_6$ are sensitive to its lattice constant [30]. For 2D $\text{Cr}_2\text{Ge}_2\text{Te}_6$, the lattice constant is 6.83 Å in the experiment [5], and becomes 6.96 Å in the optimized structure. The experimental and the calculated results with experimental and relaxed lattice constants are given in Table I. The experimental data of T_C and lattice constant for 2D $\text{Cr}_2\text{Ge}_2\text{Te}_6$ shown in Table I are taken from Ref. [5]. For the hexagonal lattice, we used the following three configurations for AFM ordering: the AFM *Néel*, AFM stripe, and AFM zigzag states [17]. The AFM state used for discussions in Table I is the AFM zigzag state, which is the lowest energy AFM state according to our calculations. In addition, for the bulk $\text{Cr}_2\text{Ge}_2\text{Te}_6$, there are some experimental reports, for example, the MAE is 0.25 meV per unit cell of $\text{Cr}_6\text{Ge}_6\text{Te}_{18}$ [47], T_C is about 66 K [47] and 62.5 K [48], and the spin moment is $3.41 \mu_B$ [48].

The MAE is defined by the energy difference of the in-plane and the out-of-plane ferromagnetic state and can be expressed as $MAE = E_{FMx} - E_{FMz}$, where E_{FMx} and E_{FMz} denote the energy of the ferromagnetic state with in-plane and out-of-plane direction of the unit cell, respectively. Our results suggest that these materials possess a ferromagnetic ground state with out-of-plane magnetization.

Our calculations show that $\text{Cr}_2\text{Ge}_2\text{Te}_6/\text{PtSe}_2$ heterostructure Stack-1 and Stack-2 are semiconductors

with finite band gaps of 0.39 and 0.45 eV, respectively. The electronic band structures and atom-projected partial density of states of Stack-1 and Stack-2 are presented in Fig. 2.

The magnetization as a function of temperature obtained by Monte Carlo simulations based on 2D Ising model is depicted in Fig. 3(a). One may note that our calculated result for T_C of monolayer $\text{Cr}_2\text{Ge}_2\text{Te}_6$ agrees well with the experimental result, revealing that our calculating method is reliable. It is shown that the Curie temperature T_C of $\text{Cr}_2\text{Ge}_2\text{Te}_6$ with 3.7% tensile strain (the lattice constant 7.22 Å) is increased beyond room temperature, and T_C of the heterostructures with Stack-1 and Stack-2 is increased above 600 K. In addition to the increase of Curie temperature, the MAE is also increased by about 40% in the $\text{Cr}_2\text{Ge}_2\text{Te}_6$ with 3.7% tensile strain, and enhanced by about 70% in the heterostructures with Stack-1 and Stack-2 as shown in Fig. 3(b). It is indicated that the MAE of Stack-1 and Stack-2 are both larger than that of $\text{Cr}_2\text{Ge}_2\text{Te}_6$ monolayer, showing that the nonmagnetic layer PtSe_2 has a remarkable effect on the enhancement of magnetism in 2D $\text{Cr}_2\text{Ge}_2\text{Te}_6$, which will be discussed in next section.

To study the effect of Hubbard parameter U on the calculated T_C and MAE, we perform DFT calculations for different values of U , as shown in Fig. 4. One may see that with increasing U , T_C of Stack-1 and Stack-2 remain almost unaltered, while T_C of monolayer $\text{Cr}_2\text{Ge}_2\text{Te}_6$ is decreasing with the increase of U . However, with increasing U the MAE is found to increase for monolayer $\text{Cr}_2\text{Ge}_2\text{Te}_6$ and heterostructure Stack-1 and Stack-2, revealing that the enhancements of T_C and MAE have different mechanisms, and electron interactions play important roles in the enhancement of MAE. In addition, the U -dependent band gap is also studied by DFT calculations. Our results show that the band gap slightly increases with increasing U in the range of 4 - 5 eV, as this is typical for 3d electrons.

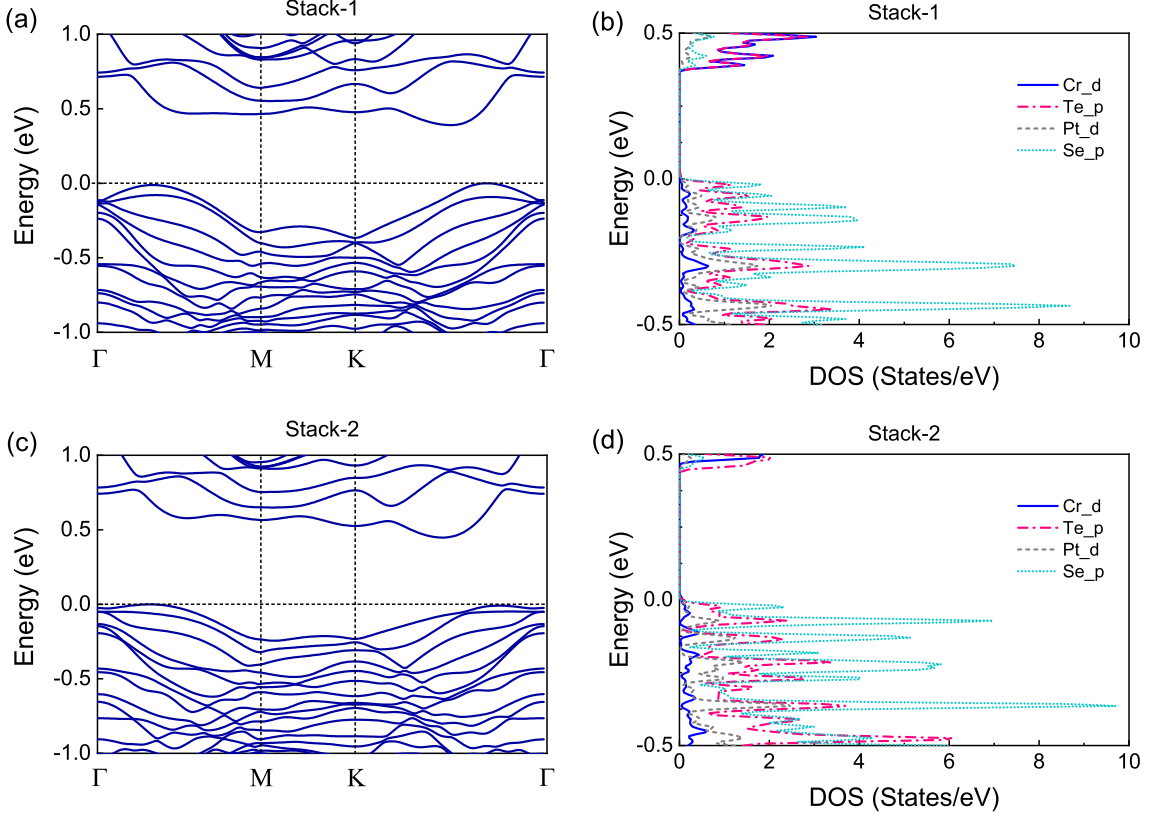


FIG. 2. Electronic band structures and partial DOS of two-dimensional $\text{Cr}_2\text{Ge}_2\text{Te}_6/\text{PtSe}_2$ heterostructures with (a), (b) Stack-1 and (c), (d) Stack-2, respectively, obtained by the GGA + SOC + U calculations with $U = 4$ eV.

IV. THEORETICAL ANALYSIS

To describe the magnetic anisotropy in monolayer $\text{Cr}_2\text{Ge}_2\text{Te}_6$ and the heterostructure $\text{Cr}_2\text{Ge}_2\text{Te}_6/\text{PtSe}_2$, we write down a general spin Hamiltonian

$$\begin{aligned}
 \hat{H}_{spin} = & \sum_{\langle i,j \rangle} J_{xx} S_{ix} S_{jx} + \sum_{\langle i,j \rangle} J_{xy} S_{ix} S_{jy} + \sum_{\langle i,j \rangle} J_{xz} S_{ix} S_{jz} \\
 & + \sum_{\langle i,j \rangle} J_{yx} S_{iy} S_{jx} + \sum_{\langle i,j \rangle} J_{yy} S_{iy} S_{jy} + \sum_{\langle i,j \rangle} J_{yz} S_{iy} S_{jz} \\
 & + \sum_{\langle i,j \rangle} J_{zx} S_{iz} S_{jx} + \sum_{\langle i,j \rangle} J_{zy} S_{iz} S_{jy} + \sum_{\langle i,j \rangle} J_{zz} S_{iz} S_{jz} \\
 & + \sum_{i,\alpha,\beta} A_{\alpha\beta} S_{i\alpha} S_{i\beta}.
 \end{aligned} \tag{1}$$

In Eq. (1), i and j denote the magnetic atom sites, and the summation on $\langle i, j \rangle$ only includes the nearest neighbors. α and β denote three directions of x , y and z axis. The former nine terms in Eq. (1) are the nearest neighbor exchange interactions between different spin components and the last term represents SIA energy. $J_{\alpha\beta}$ are the matrix elements of exchange couplings between the nearest spins, and the off-diagonal

TABLE II. The diagonal elements of exchange coupling matrix J (in units of meV) for monolayer $\text{Cr}_2\text{Ge}_2\text{Te}_6$, 2D $\text{Cr}_2\text{Ge}_2\text{Te}_6$ with 3.7% tensile strain and $\text{Cr}_2\text{Ge}_2\text{Te}_6/\text{PtSe}_2$ heterostructures calculated by the GGA + SOC + U and the four-state method [53]. Here $U = 4$ eV.

	J_{xx}	J_{yy}	J_{zz}
$\text{Cr}_2\text{Ge}_2\text{Te}_6$ -relax	-8.068	-7.467	-8.316
$\text{Cr}_2\text{Ge}_2\text{Te}_6$ -strain	-11.314	-10.591	-11.620
Stack-1	-12.557	-11.813	-12.896
Stack-2	-12.290	-11.508	-12.623

elements lead to the Kitaev interactions [13, 49] and the Dzyaloshinskii-Moriya (DM) [50–52] interactions. Matrix elements of exchange coupling matrix J of $\text{Cr}_2\text{Ge}_2\text{Te}_6$ and $\text{Cr}_2\text{Ge}_2\text{Te}_6/\text{PtSe}_2$ could be calculated by the GGA + SOC + U method and the four-state method [53], where we take, as usual, $U = 4$ eV.

To calculate parameter $J_{\alpha\beta}$, for instance, J_{xy} , the following four classical spin configurations are used [53]: $S_1 = (1, 0, 0)$, $S_2 = (0, 1, 0)$; $S_1 = (1, 0, 0)$, $S_2 = (0, -1, 0)$; $S_1 = (-1, 0, 0)$, $S_2 = (0, 1, 0)$; $S_1 = (-1, 0, 0)$, $S_2 = (0, -1, 0)$. Keep the same for the rest spins, where $S = (0, 0, 1)$ is used in our calculation. Eq. (1) with these four

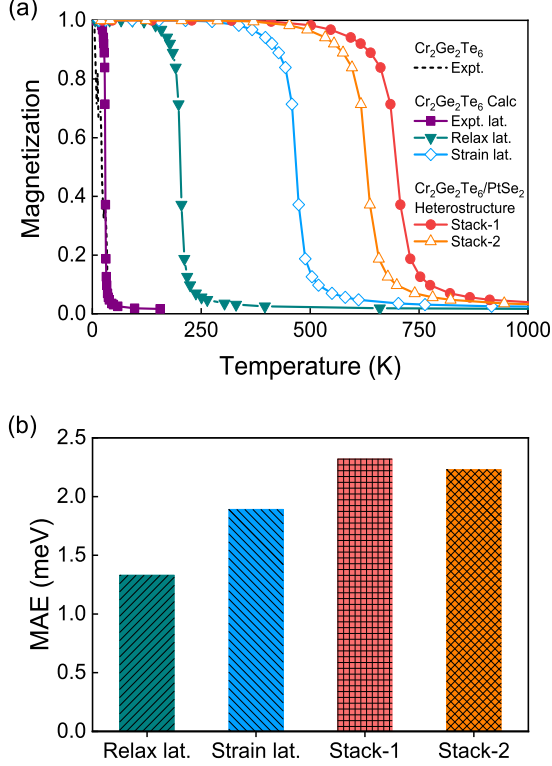


FIG. 3. For two-dimensional Cr₂Ge₂Te₆, Cr₂Ge₂Te₆ with strain, and Cr₂Ge₂Te₆/PtSe₂ heterostructures with Stack-1 and Stack-2, (a) the normalized magnetization as a function of temperature, in which Cr₂Ge₂Te₆ with experimental lattice was taken from our previous work [17] and (b) the magnetic anisotropic energy (MAE). The experimental result of Cr₂Ge₂Te₆ is taken from Ref. [5]. The calculated results are obtained by the GGA + SOC + U calculations and the Monte Carlo simulations, where $U = 4$ eV.

spin configurations can be written as

$$\begin{aligned}
 E_1 &= J_{xy}S_{1x}S_{2y} + E_0 = J_{xy}|S|^2 + E_0, \\
 E_2 &= -J_{xy}S_{1x}S_{2y} + E_0 = -J_{xy}|S|^2 + E_0, \\
 E_3 &= -J_{xy}S_{1x}S_{2y} + E_0 = -J_{xy}|S|^2 + E_0, \\
 E_4 &= J_{xy}S_{1x}S_{2y} + E_0 = J_{xy}|S|^2 + E_0.
 \end{aligned} \tag{2}$$

One has $J_{xy} = ((E_1 + E_4) - (E_2 + E_3))/4$. Other elements of J can be obtained in a similar way. The diagonal elements of J are given in Table II. The negative values mean the ferromagnetic coupling. It is clear that the ground state is ferromagnetic for these four structures. The off-diagonal elements of J and their differences of monolayer Cr₂Ge₂Te₆ and Cr₂Ge₂Te₆/PtSe₂ heterostructures are given in Table III.

The magnitude of DM interaction can be estimated as

$$D_z = \frac{|J_{yx} - J_{xy}|}{2}. \tag{3}$$

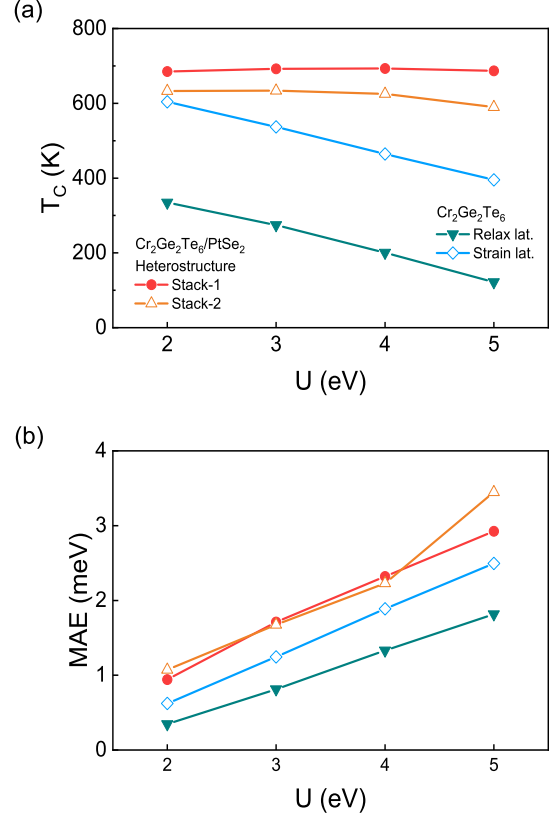


FIG. 4. The Hubbard parameter U dependence of (a) Curie temperature T_C and (b) magnetic anisotropic energy (MAE) for Cr₂Ge₂Te₆-relaxed, Cr₂Ge₂Te₆-strain (3.7%), Cr₂Ge₂Te₆/PtSe₂ heterostructures with Stack-1 and Stack-2, obtained by the GGA + SOC + U calculations.

We find that for monolayer Cr₂Ge₂Te₆, $J_{xy} = J_{yx}$, $J_{xz} = J_{zx}$, $J_{zy} = J_{yz}$, and thus there is no DM interaction. This is expected, because the inversion symmetry is kept in the monolayer. For the Cr₂Ge₂Te₆/PtSe₂ heterostructures, the difference of the off-diagonal elements are finite values, which implies the presence of DM interaction.

The other contribution to the MAE is the SIA energy, i.e. the last term in Eq. (1). For monolayer Cr₂Ge₂Te₆ with relaxation and strain, and Cr₂Ge₂Te₆/PtSe₂ heterostructure with Stack-1 and Stack-2, the SIA energy is calculated by the GGA + SOC + U method, where we assume again $U = 4$ eV. As shown in Fig. 5, the SIA energy increases from monolayer Cr₂Ge₂Te₆ to Stack-1 and Stack-2. Comparing the SIA in Fig. 5 with the MAE in Fig. 3(b), one may note that the enhancement of the SIA and MAE is very similar.

The above DM interaction and the SIA originate from the spin-orbit coupling, which in turn contribute to the MAE. For recent magnetic semiconductor monolayers, various microscopic mechanisms of MAE are also discussed [56–58].

We also calculate the second nearest neighbor exchange coupling J_2 and the nearest neighbor exchange

TABLE III. The off-diagonal elements of exchange coupling matrix J (in units of meV) for monolayer $\text{Cr}_2\text{Ge}_2\text{Te}_6$ with relaxation and strain, and $\text{Cr}_2\text{Ge}_2\text{Te}_6/\text{PtSe}_2$ heterostructures with Stack-1 and Stack-2 calculated by the GGA + SOC + U method and the four-state method [53]. Here $U = 4$ eV.

	J_{xy}	J_{yx}	J_{xz}	J_{zx}	J_{yz}	J_{zy}	$ J_{xy} - J_{yx} $	$ J_{xz} - J_{zx} $	$ J_{yz} - J_{zy} $
$\text{Cr}_2\text{Ge}_2\text{Te}_6$ -relax	-0.493	-0.493	0.069	0.069	-0.111	-0.111	0.000	0.000	0.000
$\text{Cr}_2\text{Ge}_2\text{Te}_6$ -strain	-0.593	-0.593	-0.061	-0.061	0.102	0.102	0.000	0.000	0.000
Stack-1	-0.750	-0.539	-0.053	0.228	-0.188	-0.072	0.211	0.281	0.116
Stack-2	0.669	0.628	-0.153	0.334	0.293	0.014	0.041	0.487	0.279

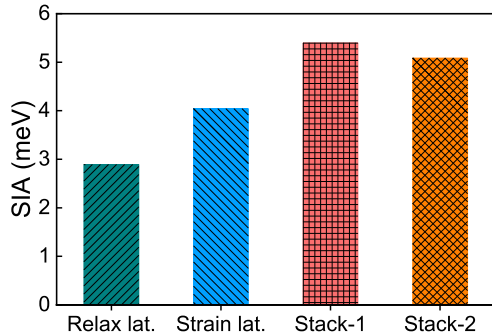


FIG. 5. The single-ion anisotropy (SIA) energy for $\text{Cr}_2\text{Ge}_2\text{Te}_6$ -relaxed, $\text{Cr}_2\text{Ge}_2\text{Te}_6$ -strain (3.7%) $\text{Cr}_2\text{Ge}_2\text{Te}_6/\text{PtSe}_2$ heterostructures with Stack-1 and Stack-2 obtained by the GGA + SOC + U calculations, with $U = 4$ eV.

coupling J_1 by comparing different magnetic configurations [54, 55]. For 2D $\text{Cr}_2\text{Ge}_2\text{Te}_6$ with relaxation, we obtain $J_1 = -8.38$ meV, $J_2 = 0.43$ meV; for 2D $\text{Cr}_2\text{Ge}_2\text{Te}_6$ with strain, $J_1 = -11.64$ meV, $J_2 = -0.06$ meV; for $\text{Cr}_2\text{Ge}_2\text{Te}_6/\text{PtSe}_2$ Stack-1, $J_1 = -13.01$ meV, $J_2 = -0.42$ meV; for $\text{Cr}_2\text{Ge}_2\text{Te}_6/\text{PtSe}_2$ Stack-2, $J_1 = -12.75$ meV, $J_2 = -0.36$ meV. Our results show that J_2 was about 20 to 30 times smaller than J_1 in magnitude in present cases. This is in contrast with the results in 2D CrI_3 , where the calculated J_2 is about 5 times smaller than J_1 in magnitude [54]. It is noted that T_C is determined by the leading term J_1 , and barely affected by small values of J_2 . Thus, the second nearest neighbor exchange coupling can be neglected in our case. Here we should mention that for the simplicity we applied an isotropic Heisenberg model to get J_1 values by comparing the energies between different magnetic configurations. Thus, the values of J_1 are approximately equal to the average of J_{xx} , J_{yy} and J_{zz} .

In fact, the above results of J_2/J_1 are consistent with the magnetic anisotropy in the experiments of 2D CrI_3 and $\text{Cr}_2\text{Ge}_2\text{Te}_6$ [5, 6]. For the 2D CrI_3 , $J_2/J_1 \sim 0.2$ was obtained in the calculation [54], and thus the DM interaction can be expected, which is consistent with the large magnetic anisotropy in 2D CrI_3 in the experiment. In contrast, for the 2D $\text{Cr}_2\text{Ge}_2\text{Te}_6$, a very small J_2/J_1

~ 0.05 was obtained in our calculation, which is also consistent with the small magnetic anisotropy in the experiment of 2D $\text{Cr}_2\text{Ge}_2\text{Te}_6$. Because the MAE in the experiment of 2D $\text{Cr}_2\text{Ge}_2\text{Te}_6$ is weak, we propose a scheme here to enhance MAE by constructing the heterostructure $\text{Cr}_2\text{Ge}_2\text{Te}_6/\text{PtSe}_2$, where the inversion symmetry is broken, and the DM interaction is expected.

V. DISCUSSION

To describe the magnetic state of 2D $\text{Cr}_2\text{Ge}_2\text{Te}_6$ and the heterostructures $\text{Cr}_2\text{Ge}_2\text{Te}_6/\text{PtSe}_2$, the Heisenberg model is used, as defined in Eq. (1). To estimate some magnetic properties, such as Curie temperature T_C and exchange parameters, the approximations with classical spins are used. For example, to calculate T_C , we carry out the Monte Carlo simulations based on the Ising model. To calculate the exchange parameters J_{xx} , J_{xy} , etc. in Eq. (1), the four-state method with four classical spin configurations are used [53].

As shown in Fig. 4(a) and (b), the Hubbard on-site Coulomb correlation U dependence of T_C and MAE are calculated. For $U = 1$ eV, our DFT results find that 2D $\text{Cr}_2\text{Ge}_2\text{Te}_6$ has a ferromagnetic ground state with in-plane magnetization (negative MAE, not shown in Fig. 4), in contrast to the experimental observation that the out-of-plane magnetization was observed. Thus, this result suggests that the small $U = 1$ eV was not reasonable for 2D $\text{Cr}_2\text{Ge}_2\text{Te}_6$. Instead, our DFT calculations suggest that a large parameter $U = 4$ eV is reasonable for 2D $\text{Cr}_2\text{Ge}_2\text{Te}_6$, where both T_C and MAE are consistent with the experimental results. In Fig. 4(a) and (b), T_C and MAE with U ranging from 2 - 5 eV are presented. It is shown that our conclusions, i.e., the great enhancement of Curie temperature and magnetic anisotropy in 2D van der Waals magnetic semiconductor heterostructures, do not change with Hubbard U in the range of 2 - 5 eV.

The great increase of T_C in $\text{Cr}_2\text{Ge}_2\text{Te}_6$ by applying tensile strain through heterostructures could be understood based on the superexchange interaction [59–61]. To deal with the superexchange interaction between the nearest neighbor Cr atoms we adopted the simple four-electron model [62]. In this model, four electrons d_1 , p , p' , d_2 are electrons of Cr, Te (contains two p electrons), and Cr atoms, respectively. The indirect magnetic interac-

TABLE IV. The DFT results of mixing-matrix $|V_{pd}|$ and energy difference $|E_p - E_d|$ between 5p orbitals of Te and 3d orbitals of Cr for $\text{Cr}_2\text{Ge}_2\text{Te}_6$ relaxed and strained (in units of eV).

$\text{Cr}_2\text{Ge}_2\text{Te}_6$ -relax					
	$p_y - d_{x^2-y^2}$	$p_y - d_{z^2}$	$p_x - d_{xy}$	$p_y - d_{yz}$	$p_z - d_{yz}$
$ V_{pd} $	0.7099	0.3583	0.3287	0.2879	0.2793
$ E_p - E_d $	0.6659	0.3525	1.1036	0.9681	1.4864
$\text{Cr}_2\text{Ge}_2\text{Te}_6$ -strain					
	$p_x - d_{xy}$	$p_y - d_{xy}$	$p_y - d_{xz}$	$p_z - d_{xy}$	$p_x - d_{yz}$
$ V_{pd} $	0.4061	0.4021	0.2960	0.2829	0.2561
$ E_p - E_d $	0.2943	0.3379	0.4141	0.3030	0.2888

tion between Cr_1 and Cr_2 can be approximately written as $J_{indirect} = [1/E(\uparrow\downarrow)^2 - 1/E(\uparrow\uparrow)^2]b^2J_{pd}$. The superexchange process could be divided into two intermediate processes. One intermediate process is the transfer of the p electron of Te to Cr_1 site, $E(\uparrow\downarrow)$ is the energy needed if spins of p and d₁ electrons form a singlet state, $E(\uparrow\uparrow)$ is the energy needed if spins of p and d₁ electrons form a triplet state, and b is the integral of this intermediate process. The other intermediate process is the direct exchange coupling between the remaining p' electron of Te and the d₂ electron of Cr_2 , where the antiferromagnetic p-d exchange coupling J_{pd} can be approximately expressed as $J_{pd} = 2|V_{pd}|^2 \frac{U}{(E_p - E_d)(E_d - E_p + U)}$ following the s-d exchange model with Schrieffer-Wolff transformation [63]. For large $U \gg |E_p - E_d|$, J_{pd} could be simplified to $J_{pd} \approx 2|V_{pd}|^2 \frac{1}{|E_p - E_d|}$. V_{pd} is the mixing matrix element between 5p orbitals of Te and 3d orbitals of Cr, and $(E_p - E_d)$ is the energy difference between 5p orbitals of Te and 3d orbitals of Cr. It is noted that both mixing term V_{pd} and energy difference $|E_p - E_d|$ are materials dependent.

By DFT calculations, we can obtain these parameters for 2D $\text{Cr}_2\text{Ge}_2\text{Te}_6$ relaxed and with a strain. The results of $|V_{pd}|$ and $|E_p - E_d|$ are listed in Table IV. Comparing the results of $\text{Cr}_2\text{Ge}_2\text{Te}_6$ with relaxation and $\text{Cr}_2\text{Ge}_2\text{Te}_6$ with strain (3.7% tensile strain), we find that the increased antiferromagnetic coupling J_{pd} by strain is mainly from the decreased energy difference $|E_p - E_d|$. The decreased $|E_p - E_d|$ gives rise to the enhanced J_{pd} , $J_{indirect}$ and T_C . There is no essential difference for the Cr-Te-Cr bond angles before and after applying the strain, where Cr-Te-Cr bond angle is 89.8 degree for $\text{Cr}_2\text{Ge}_2\text{Te}_6$ -relax, and 92.3 degree for $\text{Cr}_2\text{Ge}_2\text{Te}_6$ -strain. It is consistent with the mixing term $|V_{pd}|$ as shown in Table IV, where there is no essential difference for $|V_{pd}|$ before and after applying the strain.

As shown in Fig. 4(a), it is clear that the increased T_C between the $\text{Cr}_2\text{Ge}_2\text{Te}_6$ with relax and the $\text{Cr}_2\text{Ge}_2\text{Te}_6$ with strain are nearly U independent, which is consistent with the nearly U independent J_{pd} . For the enhanced T_C of heterostructures, as shown in Fig. 4 (a), an important contribution comes from the strain effect in the heterostructures. For the T_C in heterostructures

$\text{Cr}_2\text{Ge}_2\text{Te}_6/\text{PtSe}_2$, other contribution rather than strain also appears with $U > 2$ eV as shown in Fig. 4(a), while the reason of such contribution needs further studies.

The MAE increases with increasing U, as shown in Fig. 4(b). This behavior could be understood by the multi-orbital electron correlations. The multi-orbital Coulomb interactions between electrons with the orbitals \mathbf{m} and $-\mathbf{m}$ and spin σ is expressed as [16, 64]: $H_{m\sigma} = (U' - J_H)n_{m\sigma}n_{m\bar{\sigma}} \approx (U' - J_H)(\bar{n}^2 - \frac{1}{4}\lambda_{SO}^2 m^2 \sigma^2 (\delta n)^2)$, where U is the on-site Coulomb interactions within the same orbitals, U' is the on-site Coulomb interactions between different orbitals, and J_H demotes the Hund coupling. In the atomic limit, these parameters satisfy the relation $U = U' + 2J_H$ [65]. λ_{SO} is the SOC parameter, giving rise to the band splitting due to spin-orbit coupling. To compensate the increased energy due to the multi-orbital Coulomb interactions, the SOC will increase with increasing U. Such enhancement of SOC due to the electron correlations has been discussed in the large topological band gap [16] and the enhancement of spin Hall effect [66, 67]. Because the MAE is originated from the SOC, MAE will also increase with increasing U.

When growing two materials together, two kinds of junctions can be considered. One is the incoherent junction, where each layer of the junction keeps their original lattice constants [37], and there is little strain at the junction. Another is the coherent junction, where the lattice constant of each layer is forced to be the same, and the strain is expected at the junction. In this work, the coherent junction is considered, and the strain at the junction is found to play an important role in enhancing the magnetic anisotropy and Curie temperature of heterostructures. Our results suggest that it is better to apply the coherent junctions to manipulate the magnetic properties of heterostructures.

VI. SUMMARY

In this paper, we have proposed that the magnetic anisotropic energy (MAE) of 2D ferromagnetic semiconductor can be strongly enhanced in heterostructures with a nonmagnetic semiconductor monolayer with large spin-orbit coupling. Based on the density functional

theory calculations, we have demonstrated this idea in the bilayer heterostructure $\text{Cr}_2\text{Ge}_2\text{Te}_6/\text{PtSe}_2$. The results show that the MAE of $\text{Cr}_2\text{Ge}_2\text{Te}_6$ is enhanced by 70%, and its Curie temperature is increased to larger than 600 K far beyond room temperature. By means of a model Hamiltonian analysis, it is shown that both the Dzyaloshinskii-Moriya interaction and the single-ion anisotropy contribute to the enhancement of the MAE. Based on the superexchange picture, the great enhancement of T_C is partially attributed to the decreased energy difference between 3d orbitals of Cr and 5p orbitals of Te. Our present study gives a deeper understanding on the mechanism of enhancement of magnetism in 2D van der Waals magnetic/nonmagnetic heterostructures and will spur further experimental studies of the 2D magnetic semiconductor systems.

ACKNOWLEDGMENTS

The authors acknowledge Q. B. Yan, Z. G. Zhu, and Z. C. Wang for many valuable discussions. This paper is supported in part by the National Key R&D Program of China (Grant No. 2018YFA0305800), the Strategic Priority Research Program of the Chinese Academy of Sciences (Grant No. XDB28000000), the National Natural Science Foundation of China (Grant No.11834014), and Beijing Municipal Science and Technology Commission (Grant No. Z190011). B.G. is also supported by the National Natural Science Foundation of China (Grant No.Y81Z01A1A9), the Chinese Academy of Sciences (Grant No. Y929013EA2), the University of Chinese Academy of Sciences (Grant No. 110200M208), the Strategic Priority Research Program of Chinese Academy of Sciences (Grant No.XDB33000000),and the Beijing Natural Science Foundation (Grant No. Z190011).

-
- [1] D. Kennedy and C. Norman, What don't we know?, *Science* **309**, 75 (2005).
- [2] K. S. Burch, D. Mandrus, and J.-G. Park, Magnetism in two-dimensional van der waals materials, *Nature* **563**, 47 (2018).
- [3] J. L. Miller, Ferromagnetism found in two-dimensional materials, *Phys. Today* **70**, 16 (2017).
- [4] N. Sethulakshmi, A. Mishra, P. Ajayan, Y. Kawazoe, A. K. Roy, A. K. Singh, and C. S. Tiwary, Magnetism in two-dimensional materials beyond graphene, *Mater. Today* **27**, 107 (2019).
- [5] C. Gong, L. Li, Z. Li, H. Ji, A. Stern, Y. Xia, T. Cao, W. Bao, C. Wang, Y. Wang, Z. Q. Qiu, R. J. Cava, S. G. Louie, J. Xia, and X. Zhang, Discovery of intrinsic ferromagnetism in two-dimensional van der Waals crystals, *Nature* **546**, 265 (2017).
- [6] B. Huang, G. Clark, E. Navarro-Moratalla, D. R. Klein, R. Cheng, K. L. Seyler, D. Zhong, E. Schmidgall, M. A. McGuire, D. H. Cobden, W. Yao, D. Xiao, P. Jarillo-Herrero, and X. Xu, Layer-dependent ferromagnetism in a van der Waals crystal down to the monolayer limit, *Nature* **546**, 270 (2017).
- [7] Y. Deng, Y. Yu, Y. Song, J. Zhang, N. Z. Wang, Z. Sun, Y. Yi, Y. Z. Wu, S. Wu, J. Zhu, J. Wang, X. H. Chen, and Y. Zhang, Gate-tunable room-temperature ferromagnetism in two-dimensional Fe_3GeTe_2 , *Nature* **563**, 94 (2018).
- [8] M. Bonilla, S. Kolekar, Y. Ma, H. C. Diaz, V. Kalappattil, R. Das, T. Eggers, H. R. Gutierrez, M.-H. Phan, and M. Batzill, Strong room-temperature ferromagnetism in VSe_2 monolayers on van der waals substrates, *Nat. Nanotechnol.* **13**, 289 (2018).
- [9] D. J. O'Hara, T. Zhu, A. H. Trout, A. S. Ahmed, Y. K. Luo, C. H. Lee, M. R. Brenner, S. Rajan, J. A. Gupta, D. W. McComb, and R. K. Kawakami, Room temperature intrinsic ferromagnetism in epitaxial manganese selenide films in the monolayer limit, *Nano Lett.* **18**, 3125 (2018).
- [10] S. Zheng, C. Huang, T. Yu, M. Xu, S. Zhang, H. Xu, Y. Liu, E. Kan, Y. Wang, and G. Yang, High-temperature ferromagnetism in an Fe_3P monolayer with a large magnetic anisotropy, *J. Phys. Chem. Lett.* **10**, 2733 (2019).
- [11] J.-U. Lee, S. Lee, J. H. Ryoo, S. Kang, T. Y. Kim, P. Kim, C.-H. Park, J.-G. Park, and H. Cheong, Ising-type magnetic ordering in atomically thin FePS_3 , *Nano Lett.* **16**, 7433 (2016).
- [12] N. D. Mermin and H. Wagner, Absence of ferromagnetism or antiferromagnetism in one- or two-dimensional isotropic Heisenberg models, *Phys. Rev. Lett.* **17**, 1133 (1966).
- [13] C. Xu, J. Feng, H. Xiang, and L. Bellaiche, Interplay between Kitaev interaction and single ion anisotropy in ferromagnetic CrI_3 and CrGeTe_3 monolayers, *npj Comput. Mater.* **4**, 57 (2018).
- [14] X. Li, B. Dong, X. Sun, H. Wang, T. Yang, G. Yu, and Z. V. Han, Perspectives on exfoliated two-dimensional spintronics, *J. Semicond.* **40**, 081508 (2019).
- [15] S. Jiang, J. Shan, and K. F. Mak, Electric-field switching of two-dimensional van der Waals magnets, *Nat. Mater.* **17**, 406 (2018).
- [16] J.-Y. You, Z. Zhang, B. Gu, and G. Su, Two-dimensional room-temperature ferromagnetic semiconductors with quantum anomalous hall effect, *Phys. Rev. Appl* **12**, 024063 (2019).
- [17] X.-J. Dong, J.-Y. You, B. Gu, and G. Su, Strain-induced room-temperature ferromagnetic semiconductors with large anomalous hall conductivity in two-dimensional $\text{Cr}_2\text{Ge}_2\text{Se}_6$, *Phys. Rev. Appl* **12**, 014020 (2019).
- [18] L. Webster and J.-A. Yan, Strain-tunable magnetic anisotropy in monolayer CrCl_3 , CrBr_3 , and CrI_3 , *Phys. Rev. B* **98**, 144411 (2018).
- [19] Y. Liu, Y. Huang, and X. Duan, Van der Waals integration before and beyond two-dimensional materials, *Nature* **567**, 323 (2019).
- [20] M. Gibertini, M. Koperski, A. F. Morpurgo, and K. S. Novoselov, Magnetic 2D materials and heterostructures, *Nat. Nanotechnol.* **14**, 408 (2019).
- [21] C. Jin, E. Y. Ma, O. Karni, E. C. Regan, F. Wang, and T. F. Heinz, Ultrafast dynamics in van der Waals het-

- erostructures, *Nat. Nanotechnol.* **13**, 994 (2018).
- [22] K. S. Novoselov, A. Mishchenko, A. Carvalho, and A. H. C. Neto, 2D materials and van der Waals heterostructures, *Science* **353**, 9439 (2016).
- [23] X. Liu and M. C. Hersam, Interface characterization and control of 2D materials and heterostructures, *Adv. Mater.* **30**, 1801586 (2018).
- [24] E. Pomerantseva and Y. Gogotsi, Two-dimensional heterostructures for energy storage, *Nature Energy* **2**, 17089 (2017).
- [25] M.-Y. Li, C.-H. Chen, Y. Shi, and L.-J. Li, Heterostructures based on two-dimensional layered materials and their potential applications, *Mater. Today* **19**, 322 (2016).
- [26] P. Solís-Fernández, M. Bissett, and H. Ago, Synthesis, structure and applications of graphene-based 2D heterostructures, *Chem. Soc. Rev.* **46**, 4572 (2017).
- [27] J. Kang, J. Li, S.-S. Li, J.-B. Xia, and L.-W. Wang, Electronic structural moiré pattern effects on MoS₂/MoSe₂ 2D heterostructures, *Nano Lett.* **13**, 5485 (2013).
- [28] B. Cho, J. Yoon, S. K. Lim, A. R. Kim, D.-H. Kim, S.-G. Park, J.-D. Kwon, Y.-J. Lee, K.-H. Lee, B. H. Lee, H. C. Ko, and M. G. Hahm, Chemical sensing of 2D graphene/MoS₂ heterostructure device, *ACS Appl. Mater. Interfaces* **7**, 16775 (2015).
- [29] J. Zhang, L. Du, S. Feng, R.-W. Zhang, B. Cao, C. Zou, Y. Chen, M. Liao, B. Zhang, S. A. Yang, G. Zhang, and T. Yu, Enhancing and controlling valley magnetic response in MoS₂/WS₂ heterostructures by all-optical route, *Nat. Commun.* **10**, 4226 (2019).
- [30] C. Gong, E. M. Kim, Y. Wang, G. Lee, and X. Zhang, Multiferroicity in atomic van der Waals heterostructures, *Nat. Commun.* **10**, 2657 (2019).
- [31] Y. Zhu, X. Wang, and W. Mi, Tunable electronic structure and magnetic anisotropy of two dimensional van der Waals GeS/FeCl₂ multiferroic heterostructures, *J. Mater. Chem. C* **7**, 2049 (2019).
- [32] D. Zhong, K. L. Seyler, X. Linpeng, R. Cheng, N. Sivadas, B. Huang, E. Schmidgall, T. Taniguchi, K. Watanabe, M. A. McGuire, W. Yao, D. Xiao, K.-M. C. Fu, and X. Xu, Van der Waals engineering of ferromagnetic semiconductor heterostructures for spin and valleytronics, *Sci. Adv.* **3**, e1603113 (2017).
- [33] X.-R. Chen, W. Chen, L. B. Shao, and D. Y. Xing, Engineering chiral edge states in two-dimensional topological insulator/ferromagnetic insulator heterostructures, *Phys. Rev. B* **99**, 085417 (2019).
- [34] W. Sun, W. Wang, D. Chen, Z. Cheng, and Y. Wang, Valence mediated tunable magnetism and electronic properties by ferroelectric polarization switching in 2D FeI₂/In₂Se₃ van der Waals heterostructures, *Nanoscale* **11**, 9931 (2019).
- [35] K. Takiguchi, T. Chiba, T. Koyama, D. Chiba, M. Tanaka, *et al.*, Giant gate-controlled proximity magnetoresistance in semiconductor-based ferromagnetic–non-magnetic bilayers, *Nat. Phys.* **15**, 1134 (2019).
- [36] L. Zhang, Z. Zhou, Y. Zhang, B. Peng, W. Ren, Z.-G. Ye, and M. Liu, Tuning the magnetic anisotropy of Fe₃O₄/Pt heterostructures fabricated by atomic layer deposition with *in situ* magnetic field, *IEEE Transactions on Magnetics* **55**, 1 (2019).
- [37] A. Koma, Van der Waals epitaxy a new epitaxial growth method for a highly lattice-mismatched system, *Thin Solid Films* **216**, 72 (1992).
- [38] X. Li, M.-W. Lin, J. Lin, B. Huang, A. A. Piretzky, C. Ma, K. Wang, W. Zhou, S. T. Pantelides, M. Chi, I. Kravchenko, J. Fowlkes, C. M. Rouleau, D. B. Geohegan, and K. Xiao, Two-dimensional GaSe/MoSe₂ misfit bilayer heterojunctions by van der Waals epitaxy, *Sci. Adv.* **2**, e1501882 (2016).
- [39] A. Ghasemi, D. Kepaptsoglou, P. L. Galindo, Q. M. Ramasse, T. Hesjedal, and V. K. Lazarov, Van der Waals epitaxy through the highly lattice mismatched Cu-doped FeSe and Bi₂Te₃, *NPG Asia Mater.* **9**, e402 (2017).
- [40] A. Ciarrocchi, A. Avsar, D. Ovchinnikov, and A. Kis, Thickness-modulated metal-to-semiconductor transformation in a transition metal dichalcogenide, *Nat. Commun.* **9**, 919 (2018).
- [41] W. Chen, Z. Sun, Z. Wang, L. Gu, X. Xu, S. Wu, and C. Gao, Direct observation of van der Waals stacking-dependent interlayer magnetism, *Science* **366**, 983 (2019).
- [42] J. Li, X. Yang, Y. Liu, B. Huang, R. Wu, Z. Zhang, B. Zhao, H. Ma, W. Dang, Z. Wei, K. Wang, Z. Lin, X. Yan, M. Sun, B. Li, X. Pan, J. Luo, G. Zhang, Y. Liu, Y. Huang, X. Duan, and X. Duan, General synthesis of two-dimensional van der Waals heterostructure arrays, *Nature* **579**, 368 (2020).
- [43] G. Kresse and J. Furthmüller, Efficient iterative schemes for *ab initio* total-energy calculations using a plane-wave basis set, *Phys. Rev. B* **54**, 11169 (1996).
- [44] S. Grimme, Semiempirical GGA-type density functional constructed with a long-range dispersion correction, *J. Comput. Chem.* **27**, 1787 (2006).
- [45] J. Liu, Q. Sun, Y. Kawazoe, and P. Jena, Exfoliating biocompatible ferromagnetic Cr-trihalide monolayers, *Phys. Chem. Chem. Phys.* **18**, 8777 (2016).
- [46] V. Carteaux, D. Brunet, G. Ouvrard, and G. Andre, Crystallographic, magnetic and electronic structures of a new layered ferromagnetic compound Cr₂Ge₂Te₆, *J. Phys.: Condens. Matter* **7**, 69 (1995).
- [47] J. Zeisner, A. Alfonsov, S. Selzer, S. Aswartham, M. P. Ghimire, M. Richter, J. van den Brink, B. Buchner, and V. Kataev, Magnetic anisotropy and spin-polarized two-dimensional electron gas in the van der Waals ferromagnet Cr₂Ge₂Te₆, *Phys. Rev. B* **99**, 165109 (2019).
- [48] Y. Liu and C. Petrovic, Critical behavior of quasi-two-dimensional semiconducting ferromagnet Cr₂Ge₂Te₆, *Phys. Rev. B* **96**, 054406 (2017).
- [49] N. Janša, A. Zorko, M. Gomilšek, M. Pregelj, K. W. Krmer, D. Biner, A. Biffin, C. Regg, and M. Klanjšek, Observation of two types of fractional excitation in the Kitaev honeycomb magnet, *Nat. Phys.* **14**, 786 (2018).
- [50] A. Fernández-Pacheco, E. Vedmedenko, F. Ummelen, R. Mansell, D. Petit, and R. P. Cowburn, Symmetry-breaking interlayer Dzyaloshinskii–Moriya interactions in synthetic antiferromagnets, *Nat. Mater.* **18**, 679 (2019).
- [51] A. Hrabec, N. A. Porter, A. Wells, M. J. Benitez, G. Burnell, S. McVitie, D. McGrouther, T. A. Moore, and C. H. Marrows, Measuring and tailoring the Dzyaloshinskii–Moriya interaction in perpendicularly magnetized thin films, *Phys. Rev. B* **90**, 020402 (2014).
- [52] S. Shi, S. Liang, Z. Zhu, K. Cai, S. D. Pollard, Y. Wang, J. Wang, Q. Wang, P. He, J. Yu, G. Eda, G. Liang, and H. Yang, All-electric magnetization switching and dzyaloshinskii–moriya interaction in WTe₂/ferromagnet heterostructures, *Nat. Nanotechnol.* **14**, 945 (2019).

- [53] H. Xiang, C. Lee, H.-J. Koo, X. Gong, and M.-H. Whangbo, Magnetic properties and energy-mapping analysis, *Dalton Trans.* **42**, 823 (2013).
- [54] V. K. Gudelli and G.-Y. Guo, Magnetism and magneto-optical effects in bulk and few-layer CrI₃: a theoretical GGA + U study, *New J. Phys.* **21**, 053012 (2019).
- [55] N. Sivadas, S. Okamoto, X. Xu, C. J. Fennie, and D. Xiao, Stacking-dependent magnetism in bilayer CrI₃, *Nano Lett.* **18**, 7658 (2018).
- [56] T. Olsen, Theory and simulations of critical temperatures in CrI₃ and other 2D materials: easy-axis magnetic order and easy-plane Kosterlitz–Thouless transitions, *MRS Communications* **9**, 1142 (2019).
- [57] S. Biswas, Y. Li, S. M. Winter, J. Knolle, and R. Valentí, Electronic properties of RuCl₃ in proximity to graphene, *Phys. Rev. Lett.* **123**, 237201 (2019).
- [58] Y. Liu and C. Petrovic, Anisotropic magnetic entropy change in Cr₂X₂Te₆ (X = Si and Ge), *Phys. Rev. Materials* **3**, 014001 (2019).
- [59] J. B. Goodenough, Theory of the role of covalence in the perovskite-type manganites [La, M(II)]MnO₃, *Phys. Rev.* **100**, 564 (1955).
- [60] J. Kanamori, Crystal distortion in magnetic compounds, *J. Appl. Phys.* **31**, S14 (1960).
- [61] P. W. Anderson, New approach to the theory of superexchange interactions, *Phys. Rev.* **115**, 2 (1959).
- [62] K.-M. Qian, D.-Sh. Dai, *Ferromagnetism: Volume I*, (Science Press, 2017) pp. 193–198.
- [63] J. R. Schrieffer and P. A. Wolff, Relation between the Anderson and Kondo Hamiltonians, *Phys. Rev.* **149**, 491 (1966).
- [64] M. C. Nguyen, Y. Yao, C.-Z. Wang, K.-M. Ho, and V. P. Antropov, Magnetocrystalline anisotropy in cobalt based magnets: a choice of correlation parameters and the relativistic effects, *J. Phys.: Condens. Matter* **30**, 195801 (2018).
- [65] S. Maekawa, Introduction, in *Physics of Transition Metal Oxides* (Springer Berlin Heidelberg, Berlin, Heidelberg, 2004) pp. 1–35.
- [66] B. Gu, J.-Y. Gan, N. Bulut, T. Ziman, G.-Y. Guo, N. Nagaosa, and S. Maekawa, Quantum renormalization of the Spin Hall effect, *Phys. Rev. Lett.* **105**, 086401 (2010).
- [67] G.-Y. Guo, S. Maekawa, and N. Nagaosa, Enhanced Spin Hall effect by resonant skew scattering in the orbital-dependent Kondo effect, *Phys. Rev. Lett.* **102**, 036401 (2009).